Electrochemical Characterization of Thin Film Electrodes Toward Developing a DNA Transistor

ARTICLE *in* LANGMUIR · DECEMBER 2010

Impact Factor: 4.46 · DOI: 10.1021/la102671g · Source: PubMed

12 AUTHORS, INCLUDING:

Stefan Harrer
IBM
47 PUBLICATIONS **339** CITATIONS
SEE PROFILE

Shafaat Ahmed
IBM
40 PUBLICATIONS **641** CITATIONS
SEE PROFILE

Lili Deligianni
IBM
9 PUBLICATIONS **107** CITATIONS
SEE PROFILE

Gustavo Stolovitzky
IBM
176 PUBLICATIONS **9,161** CITATIONS
SEE PROFILE

Langmuir
Article
pubs.acs.org/Langmuir

Electrochemical Characterization of Thin Film Electrodes Toward Developing a DNA Transistor

Stefan Harrer,* Shafaat Ahmed, Ali Afzali-Ardakani, Binquan Luan, Philip S. Waggoner, Xiaoyan Shao, Hongbo Peng, Dario L. Goldfarb, Glenn J. Martyna, Stephen M. Rossnagel, Lili Deligianni, and Gustavo A. Stolovitzky

IBM T. J. Watson Research Center, 1101 Kitchawan Road, Yorktown Heights, New York 10598, United States

Received July 7, 2010. Revised Manuscript Received November 7, 2010

The DNA-Transistor is a device designed to control the translocation of single-stranded DNA through a solid-state nanopore. Functionality of the device is enabled by three electrodes exposed to the DNA-containing electrolyte solution within the pore and the application of a dynamic electrostatic potential well between the electrodes to temporarily trap a DNA molecule. Optimizing the surface chemistry and electrochemical behavior of the device is a necessary (but by no means sufficient) step toward the development of a functional device. In particular, effects to be eliminated are (i) electrochemically induced surface alteration through corrosion or reduction of the electrode surface and (ii) formation of hydrogen or oxygen bubbles inside the pore through water decomposition. Even though our motivation is to solve problems encountered in DNA transistor technology, in this paper we report on generic surface chemistry results. We investigated a variety of electrode−electrolyte−solvent systems with respect to their capability of suppressing water decomposition and maintaining surface integrity. We employed cyclic voltammetry and long-term amperometry as electrochemical test schemes, X-ray photoelectron spectroscopy, atomic force microscopy, and scanning, as well as transmission electron microscopy as analytical tools. Characterized electrode materials include thin films of Ru, Pt, nonstoichiometric TiN, and nonstoichiometric TiN carrying a custom-developed titanium oxide layer, as well as custom-oxidized nonstoichiometric TiN coated with a monolayer of hexadecylphosphonic acid (HDPA). We used distilled water as well as aqueous solutions of poly(ethylene glycol) (PEG-300) and glycerol as solvents. One millimolar KCl was employed as electrolyte in all solutions. Our results show that the HDPA-coated custom-developed titanium oxide layer effectively passivates the underlying TiN layer, eliminating any surface alterations through corrosion or reduction within a voltage window from −2 V to +2 V. Furthermore, we demonstrated that, by coating the custom-oxidized TiN samples with HDPA and increasing the concentration of PEG-300 or glycerol in aqueous 1 mM KCl solutions, water decomposition was suppressed within the same voltage window. Water dissociation was not detected when combining custom-oxidized HDPA-coated TiN electrodes with an aqueous 1 mM KCl−glycerol solution at a glycerol concentration of at least 90%. These results are applicable to any system that requires nanoelectrodes placed in aqueous solution at voltages that can activate electrochemical processes.

I. Introduction

Employing solid nanopores for detection of whole DNA molecules has been successfully demonstrated by several groups.[2−4] All these approaches enable DNA detection with a resolution of not less than approximately 10−15 nucleotides.[4] A number of methods for nucleobase identification using nanopores have been proposed recently.[5] One such method is the use of a nanopore in combination with DNA-induced current signals for reading out specific nucleotide sequences as the DNA molecule is pulled through the pore. However, these methods have not been brought to practice in a nanopore yet due to (i) limited fabrication capabilities for a suitable nanopore device, (ii) lack of means to sufficiently slow down DNA translocation inside the pore, and (iii) lack of sufficient control of the DNA molecule while it translocates.[5] We have previously introduced a device capable of base-by-base ratcheting of single-stranded DNA through a solid-state nanopore, which we call DNA-Transistor.[1,7] In this device, DNA-trapping is enabled by generating a potential well inside the nanopore along its longitudinal direction temporarily trapping the negatively charged ssDNA in a predefined position. Three electrodes located inside the pore are used to create an electrostatic potential well. DNA is solved in an aqueous electrolyte solution and pulled into the pore by introducing an external constant potential drop between the two reservoirs on each side of the pore. Pore diameters are typically on the order of 3−5 nm. The two core requirements for maintaining our device functionality are that the pore (i) remains unaltered and operational as well as (ii) unobstructed during device operation. Hence, corrosion or reduction effects on electrode surfaces as well as bubble formation through water decomposition inside the pore must be minimized.

*Corresponding author. E-mail: sharrer@us.ibm.com. Phone: +1-914-945-2535.

(1) Polonsky, S.; Rossnagel, S.; Stolovitzky, G. Nanopore in metal-dielectric sandwich for DNA position control. *Appl. Phys. Lett.* **2007**, *91*, 153103−1–153103−3.

(2) Kasianowicz, J. J.; Brandin, E.; Branton, D.; Deamer, D. W. Characterization of individual polynucleotide molecules using a membrane channel. *Proc. Natl. Acad. Sci. U.S.A.* **1996**, *93*, 13770–13773.

(3) Braha, O.; et al. Designed protein pores as components for biosensors. *Chem. Biol.* **1997**, *4*, 497–505.

(4) Meller, A.; Nivon, L.; Brandin, L.; Golovchenko, E.; Branton, D. Voltage-driven DNA translocations through a nanopore. *Phys. Rev. Lett.* **2001**, *86*, 3435–3438.

(5) Branton, D.; et al. The potential and challenges of nanopore sequencing. *Nat. Biotechnol.* **2008**, *26*, 1146–1153.

(6) Bard, A. J.; Parsons, R.; , Jordan, J. *Standard potentials in aqueous solution*, 1st ed.; CRC Press: Boca Raton, 1985; ISBN 0−8247−7291−1.

(7) Peng, H.; Polonsky, S.; Stolovitzky, G.; Luan, B.; Martyna, G.; , Rossnagel, S. Solid-state nanopore with multiple embedded circular addressable electrodes, submitted for publication, April 2010.

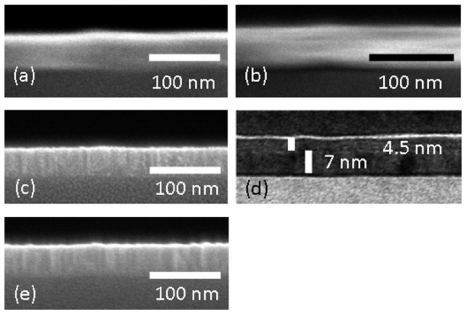

Figure 1. SEM and TEM cross-section images of test samples, in detail: (a) Ru test sample (SEM), (b) Pt test sample (SEM), (c) type 1 TiN test sample (SEM), (d) HDPA-coated type 2 TiN test sample comprising a 4.5-nm-thick titanium oxide layer on top of a 7-nm-thick TiN layer (TEM), and (e) an HDPA-coated type 1 TiN test sample (SEM). The continuous bright line (d) visible on top of the titanium oxide layer shows a chromium oxide layer added during TEM sample preparation.

This paper provides electrochemical analyses of selected electrode−electrolyte−solvent systems with special focus on their capability to suppress water decomposition and maintain surface integrity in operational mode. We want to emphasize that this work is a significant step in controlling the electrochemistry not only of a DNA-transistor (our primary motivation), but also of other devices incorporating nanometer-scale electrodes exposed to electrolyte−solvent solutions such as, for example, nanowires, electroplated surfaces, cell-on-a-chip devices, and biosensors. Section II gives a detailed description of custom-developed electrode sample preparation processes. Experimental design including corresponding measurement techniques is introduced in section III. Experimental results are discussed in section IV. Finally, an electrode−electrolyte−solvent system for which corrosion and water decomposition were undetected under the electrochemical working conditions of a DNA-Transistor is presented in section V.

II. Electrode Sample Preparation

We used silicon wafers carrying a 200-nm-thick SiO_2 layer as sample substrate for all electrode samples. In a first step, thin films of thicknesses ranging from 4.5 to 70 nm to be tested were deposited onto the substrate according to the process descriptions given in subsections A and B below.

In a second step, the wafer was precision diced into 6.5 mm × 6.5 mm square-shaped samples, and in a third step, the diced samples were cleaned in an ultrasonic acetone bath followed by ozone treatment through UV-exposure. Selected samples were then coated with a protective organic monolayer in an optional fourth step following the process laid out in subsection C below.

A. Thin Film Deposition. We tested thin films of Ru (layer thickness approximately 70 nm, Figure 1a), Pt (layer thickness approximately 65 nm, Figure 1b), nonstoichiometric TiN, and nonstoichiometric TiN carrying a custom-developed titanium oxide layer, as well as custom-oxidized nonstoichiometric TiN coated with a monolayer of hexadecylphosphonic acid (HDPA). Pt and Ru are widely used as materials for inert electrodes. However, nanoscopic corrosion effects may occur under unfavorable conditions. Corresponding chemical reactions and their standard redox potentials are given in ref 6. We investigate potential nanoscopic corrosion effects on the above metals and determine conditions under which corrosion does not occur.

Ru films ($P_{working}$ = 0.8 mT, power = 500 W, time = 180 s) and TiN films were deposited using an Endura 200 mm rotating-magnet magnetron (Applied Materials). Pt films ($P_{working}$ = 0.8 mT, power = 1 kW, time = 360 s) were deposited employing an Endura 150 mm rotating-magnet magnetron (Applied Materials).

Two types of nonstoichiometric TiN samples were prepared: Type 1 samples comprised a TiN layer thickness of 65 nm (reactive-sputter-deposition, $P_{working}$ = 1.0 mT, flow = 75% Ar, 25% N_2, power = 2.5 kW, time = 390 s; Figure 1c). Type 2 samples had a TiN layer thickness of 7 nm (Figure 1d). Other inert metals such as, for example, gold or Al-coated ZnO (AZO) may have favorable electrochemical properties but do not withstand the high-deposition temperatures necessary for building up dielectric layers in a DNA-Transistor device,[7] and were therefore not tested.

B. TiN Oxidation. All type 2 TiN samples were custom-oxidized in an O_2 plasma treatment step ($P_{working}$ = 150 mT, flow = 100 sccm, power = 40−200 W, time = 0−80 s) using an Unaxis 950 series etch chamber yielding a 4.5-nm-thick titanium oxide layer on top of the 7-nm-thick TiN layer. AFM surface roughness measurements as well as TEM cross-section imaging reveal that both the TiN layer and the capping titanium oxide layer are extremely uniform and have a constant thickness distribution across the complete sample surface area (Figure 1d and Figure 3). We can control the thickness of the titanium oxide layer with subnanometer precision down to a minimum thickness of 0.9 Å.

It is important to emphasize that this oxidation process can be not only applied to planar surfaces, but also to topographically patterned surfaces isotropically oxidizing angled and vertical sidewalls as can, for example, be found inside a nanopore.

C. Protective Organic Coating. Several type 1 and type 2 TiN samples were additionally coated with long-chain organic phosphonic acids and hydroxamic acids forming highly compact self-assembled monolayers on the titanium oxide surface of the TiN electrodes.

Long-chain phosphonic acids (R-PO_3H_2) where R can be alkyl chains of 1−18 carbons are self-assembled on the titanium oxide surface, which renders the surface completely hydrophobic. The same can be accomplished using alkylhydroxamic acids (R-CONHOH), where again R can be alkyl chains of C1 to C18 chain length. In both cases, self-assembly of these materials is carried out in dilute solution of these compounds in an organic solvent like ethanol. The alkyl chains of phosphonic or hydroxamic acids can also be partially or fully fluorinated to impart yet higher hydrophobicity on the titanium oxide surface of the electrodes. In this report, we show results for coating titanium oxide surfaces with hexadecylphosphonic acid (HDPA, chain length C16, monolayer thickness approximately 2 nm).

We investigated HDPA-coating uniformity on type 2 TiN samples by means of X-ray photoelectron spectroscopy (XPS), AFM surface roughness measurements, and chemical surface angle tests. Existing XPS reference data of an HfO_2 sample coated with an HDPA-monolayer was compared to XPS data of a type 2 TiN sample processed as described above. Results indicate that type 2 TiN samples carry a uniform HDPA-monolayer covering the complete titanium oxide surface area (Figure 2). AFM measurements were taken from various locations across the electrode sample surface and show that HDPA coating does not seem to alter the surface roughness of the TiO_2 layer underneath (Figure 3). Finally, surface angle tests confirmed the hydrophobic character of the HDPA-coated surface.

The described coating process can be performed on planar surfaces as well as inside nanopores.[8]

(8) Wanunu, M.; Meller, A. Chemically modified solid-state nanopores. *Nano Lett.* **2007**, *7*(6), 1580–1585.

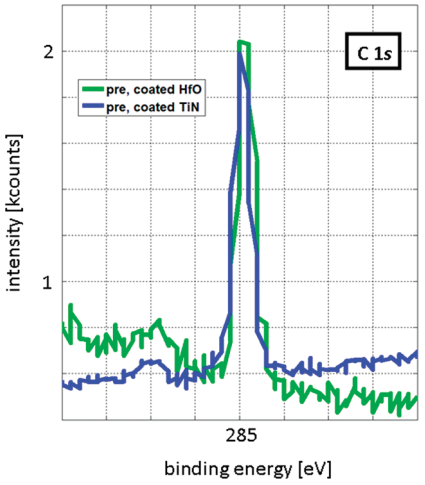

Figure 2. High-resolution C 1s XPS spectra comparing reference data of a plasma-oxidized HfO_2 sample coated with a highly uniform HDPA monolayer (green) with data obtained from a type 2 TiN test sample coated with HDPA (blue). The intensities of the C 1s peaks in both spectra are essentially the same, indicating that our coating process yields a highly uniform HDPA monolayer on our custom-oxidized type 2 TiN test samples.

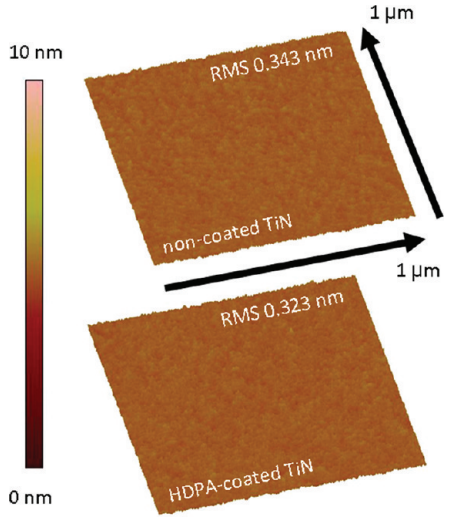

Figure 3. AFM surface roughness comparison of noncoated type 2 TiN samples and type 2 TiN samples covered with an HDPA monolayer. The measurements show that the titanium oxide surface is very smooth (top) and that HDPA-coating preserves the low surface roughness (bottom).

III. Computations and Experiments

A. Simulation of the Device and Selection of Voltage Window. All-atom molecular dynamics (MD) simulations show that single-stranded DNA (ssDNA) can be base-by-base ratcheted through a solid-state nanopore in a controlled manner under realistic dynamical operating conditions of a DNA-Transistor.[9] On the basis of these results and the device dimension requirements laid out in ref 1, we have simulated a specific device design comprising a pore diameter of 4 nm and three TiN electrodes (each of thickness $2d$) separated by two dielectric layers (each of thickness $2.5d$), where d, the spacing between two neighboring phosphate groups on the backbone of a stretched ssDNA molecule, is taken

(9) Luan, B.; Peng, H.; Polonsky, S.; Rossnagel, S.; Stolovitzky, G.; Martyna, G. Base-by-base ratcheting of single-stranded DNA through a solid-state nanopore. *Phys. Rev. Lett.* **2010**, *104*(23), 238103−1–238103−4.

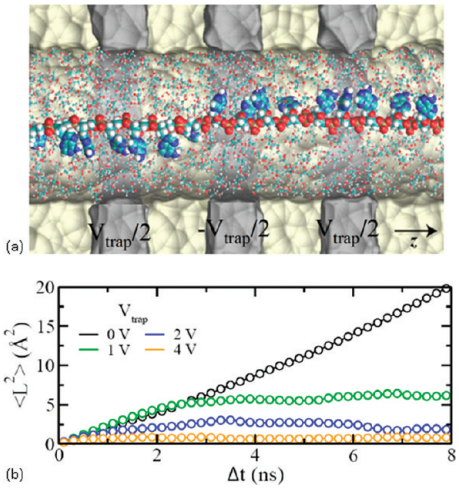

Figure 4. Full-atom molecular dynamics (MD) simulations of ssDNA moving in a DNA-Transistor show that DNA can be successfully trapped within a potential barrier V_{trap} of approximately 4 V inside the nanopore: (a) Schematics of the DNA-Transistor and simulation setup. The 4 V potential barrier is implemented by applying −2 V to the central electrode and 2 V to the side electrodes, these voltages being relative to a reference electrode in contact with the electrolyte and (b) mean square displacement of a DNA molecule. An aqueous 50% glycerol solution containing KCl as electrolyte was used as DNA solvent in all simulations. The 4 V potential trapping window V_{trap} is an integral part of all electrochemical test schemes presented in this paper.

to be 7.4 Å. ssDNA is simulated to be dissolved in an aqueous 50% glycerol solution containing KCl as electrolyte (Figure 4a). Simulation results for DNA trapping efficiency vs trapping voltage are presented in Figure 4b: a voltage drop of 4 V between adjacent electrodes is sufficient to efficiently trap the DNA molecule and temporarily hold it against thermal motion in order to facilitate single-base readout. In order to minimize surface reactivity on the electrode surfaces inside the pore, it is essential to minimize the applied absolute voltage levels. Hence, the optimum potential configuration yielding a dynamic 4 V net potential drop can be implemented by setting the center electrode to −2 V and both outer electrodes to +2 V, with these voltages being applied relative to a reference electrode in contact with the electrolyte. Note that it is not necessary to apply a voltage of 4 V to any electrode inside the DNA-Transistor at any time during operational mode in order to create the required 4 V trapping potential. Instead, switching electrode potentials back and forth in a controlled manner between a minimum applied voltage of −2 V and a maximum applied voltage +2 V allows for generating a total potential drop of 4 V between the electrodes.

These computational results indicate the feasibility of the device. They also indicate the need to test the electrochemistry within a voltage window of −2 V to +2 V.

All electrode samples and electrolyte−solvent systems were tested within a −2 V to +2 V voltage window. Custom-designed experimental electrochemical test schemes are explained in the following subsections B and C below.

B. Cyclic Voltammetry. We used cyclic voltammetry (CV) primarily to obtain data on total surface reactivity in various electrolyte−electrode systems without breaking CV data down into specific reactions. However, in selected cases we assigned specific chemical reactions to characteristic sections of obtained cyclic voltamogramms by (i) determining which reactants were present, (ii) determining redox standard potentials for all possible

reactions, and (iii) relating characteristic parts of the cyclic voltamogramm to these redox potentials.

Cyclic voltammetry was performed using a three-electrode cell[10] incorporating a platinum mesh counter electrode, a custom-built rotating-disk working electrode (Pine Research Instrumentation, Raleigh, NC, USA) carrying the test samples, an Ag|AgCl|10% KNO_3 reference electrode (Pine Research Instrumentation), and a CHI 660D potentiostat (CH Instruments, Austin, TX, USA). Measured surface current density data was 3σ noise filtered and then fitted by cubical interpolation using *Matlab* data postprocessing software. "Surface current density" and "surface reactivity" are used as synonyms in this article. For all experiments presented in this paper, all reported voltages are given with respect to the reference electrode.

When employing CV to study electrode behavior in different electrolyte−solvent systems, it is essential to create the same diffusion layer conditions, namely, the same diffusion-limiting current density at the surface of the rotating electrode test sample for each electrolyte−solvent system. The diffusion-limiting current density i_{limit} of a rotating disk electrode (RDE) in an aqueous electrolyte−solvent system can be calculated using the Levich equation[11,12]

$$i_{limit} = 0.62nFD^{2/3}\upsilon^{-1/6}\omega^{1/2}C \quad (1)$$

with

$$D = kT/6\pi\eta r_0 \quad (2)$$

and

$$\eta = \rho\upsilon \quad (3)$$

(n = number of transfer valence electrons, F = Faraday constant, C = solvent concentration in aqueous solution, υ = kinematic viscosity, ω = rotation rate, D = diffusion coefficient of involved ions, r_0 = radius of diffusion species, η = viscosity of solution, ρ = density of solution). Electrode test samples mounted to the working RDE must have exactly the same surface area for the above equations to hold. We ensure this by precision-dicing all test samples after thin film deposition as described in section II above. For two different solutions containing the same electrolyte (in our experiments always 1 mM KCl), the only variables left when equating i_{limit} are then kinematic viscosity υ, density ρ, and rotation rate ω

$$(\rho_1)^{-2/3}(\upsilon_1)^{-5/6}(\omega_1)^{1/2} = (\rho_2)^{-2/3}(\upsilon_2)^{-5/6}(\omega_2)^{1/2} \quad (4)$$

Density and viscosity are solution inherent parameters and thus not externally adjustable in our experimental setup. Hence, the only parameter left for adjusting i_{limit} for two given solutions comprising different densities and kinematic viscosities but containing the same electrolyte is the rotation rate ω according to

$$\omega_2 = (\rho_1/\rho_2)^{-4/3}(\upsilon_1/\upsilon_2)^{-5/3}\omega_1 \quad (3.5)$$

Hereby, ω_1 serves as reference rotation rate for an initial solution (ρ_1, υ_1) and has to be chosen in such a way that the corresponding adjusted rotation rates $\omega_{2,i}$ for all solutions to be compared to each other ($\rho_{2,i}$, $\upsilon_{2,i}$) do not exceed the rotation speed of the RDE controller. In our setup, the maximum rotation speed of the RDE unit was 10 krpm. Therefore, we chose the reference rotation rates as follows: for CV experiments involving aqueous glycerol and PEG-300 solutions, the reference rotation rate $\omega_{1,glycol/PEG}$ was 1 krpm, the corresponding initial solution ($\rho_{1,PEG}$, $\upsilon_{1,PEG}$) was 1 mM KCl 100% PEG-300 solution. The reference rotation rate $\omega_{1,water}$ for CV experiments involving exclusively 1 mM KCl DI water as initial solution was 0.56 krpm. All necessary viscosities were determined as explained in subsection IV.B below.

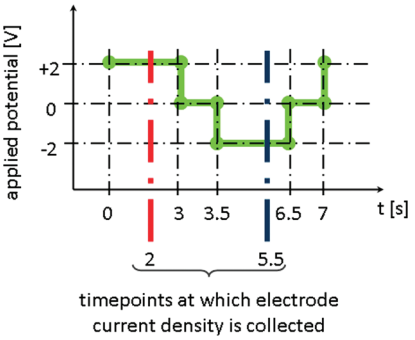

Figure 5. One cycle (7 s) of a multi(4)-step amperometry test scheme comprising step 1 (2 V, 3 s), step 2 (0 V, 0.5 s), step 3 (−2 V, 3 s), and step 4 (0 V, 0.5 s). 7200 cycles were continuously carried out subsequently during one MSA test experiment simulating a DNA-Transistor in long-term operational mode.

C. Single- and Multistep Amperometry. Using the cell and potentiostat described in subsection B above, we also performed multistep amperometry (MSA) and single-step amperometry (SSA) test schemes. While a constant voltage is applied to the electrode test sample mounted to the RDE in SSA, MSA exposes the test sample to multiple voltage steps during a test run. Surface current density was measured at a constant rate over time in SSA and at selected points of time during the step sequence in MSA.

Figure 5 illustrates the MSA test scheme we designed to mimic operating conditions of a DNA-Transistor device according to our simulation results as laid out in subsection III.A above. The RDE was not rotating during MSA and SSA tests to mimic operation conditions in the DNA-Transistor.

D. AFM Analysis. We measured the surface roughness of electrode samples by scanning over 1 μm × 1 μm square-shaped test fields on the surface of tested samples using a Dimension-3000 atomic force microscope (Veeco) operated in tapping mode. Probe tips comprised tip diameters ranging from 5 to 10 nm.

E. XPS Analysis. XPS analyses were performed using a PHOIBUS-100 spectrometer employing a SPECS hemispherical analyzer with the spectrometer arranged in the normal direction with respect to the sample surface. XPS data were generated without a monochromator using Al Kα X-rays (power = 200 W) comprising a kinetic energy of 1486 eV. High-resolution spectra were measured at pass energies of 20−50 eV. Measurement data was 3σ noise filtered and then fitted by square interpolation using *Matlab* data postprocessing software.

Natural C 1s hydrocarbon deposition on all electrode samples at 284.6 eV (sp^2, graphite) and 285 eV (sp^3, aliphatic contamination)[13] could be minimized by analyzing all samples right after processing, yielding a spectral carbon saturation intensity of approximately 0.6 kcounts. This natural carbon layer is present on each sample and causes the same signal attenuation in each XPS

(10) Kissinger, P. T.; Heinemann, W. R. Cyclic Voltammetry. *J. Chem. Educ.* **1983**, *60*(9), 702–706.

(11) Gasteiger, H. A.; Marcovic, N. M.; Ross, P. N., Jr. H2 and CO electrooxidation on well- characterized Pt, Ru, and Pt-Ru. 1. Rotating disk electrode studies of the pure gases including temperature effects. *J. Phys. Chem.* **1995**, *99*, 8390–8301.

(12) Bard, A. J.; Faulkner, L. R. *Electrochemical methods: fundamentals and applications*, 2nd ed.; John Wiley & Sons: New York, 2000; ISBN 0471043729; p 339.

(13) Kirchner, C. N.; Hallmeier, K. H.; Szargan, R.; Raschke, T.; Radehaus, C.; Wittstock, G. Evaluation of thin film titanium nitride electrodes for electroanalytical applications. *Electroanalysis* **2001**, *19*, 1023–1031.

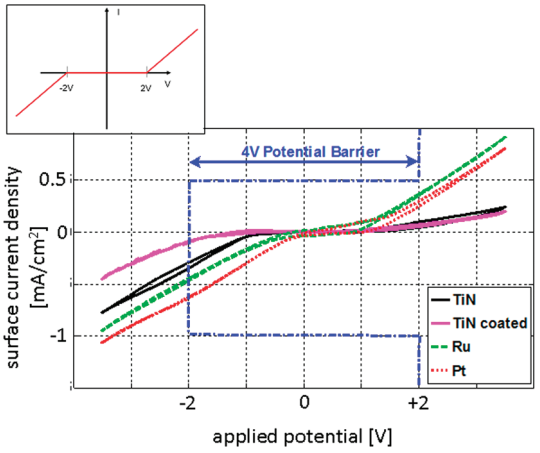

Figure 6. *V*−*I* curves for several electrode materials in 1 mM KCl DI water solution. Each color displays one CV cycle with a voltage sweep of −3.5 V to +3.5 V. The 4 V potential barrier for confining the negatively charged DNA molecule between the electrodes of the DNA-Transistor is indicated by a blue dash−dotted line. Ru, Pt, and noncoated type 1 TiN samples develop high surface reactivity within the complete barrier region and beyond. HDPA-coated type 1 TiN samples show the lowest surface reactivity. The inset on top schematically shows the ideal *V*−*I* characteristics of the system for the DNA-Transistor application.

spectrum. All spectra were calibrated with respect to the residual 0.6 kcounts C 1s peak.

F. TEM Analysis—Cross-Section Measurements. Electrode test samples were prepped using a FEI 200 TEM focused ion beam (FIB) tool and then imaged on a FEI CM12 TEM. Bright field diffraction contrast and dark field imaging conditions were used. Before FIB milling, chromium was sputter-coated onto the surface of all test samples generating a nonuniform, approximately 1-nm-thick chromium oxide layer on the surface of most imaged samples.

IV. Results and Discussion

Choosing material and design parameters of the electrode thin film impacts both the degree of possible corrosion of the electrode and the intensity of electrochemical dissociation of the solvent occurring at its surface. Both effects are directly linked to surface reactivity for a specific solvent, which in turn depends on the electrode material. The solvent material primarily determines the intensity of electrochemical dissociation and hence the rate of bubble formation in the solution. Reference 6 provides corresponding standard redox potentials.

A. Electrode Optimization. In a first step, we tested Ru, Pt, and noncoated as well as HDPA-coated type 1 TiN samples in a 1 mM KCl DI water solution using CV (5 cycles, voltage sweep −3.5 V to +3.5 V, ramping rate 0.1 V/s, RDE 0.556 krpm). Our results (Figure 6) clearly point toward TiN as preferred electrode material showing the lowest surface reactivity of all tested materials. However, HDPA-coated as well as noncoated type 1 TiN samples showed clear evidence of surface corrosion (Figure 7). All cyclic voltamogramms of Figure 6 comprise shapes that are characteristic for water dissociation reactions on the surface of inert electrodes. Pt and Ru are known to catalyze electrochemical dissociation of water,[14,15] which can also be observed in the

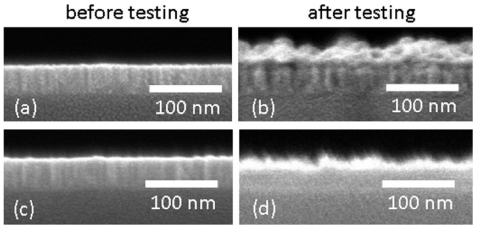

Figure 7. SEM cross-section images of (a) a noncoated type 1 TiN sample before CV testing, (b) the same sample after CV testing (−3.5 V to +3.5 V), (c) a HDPA-coated type 1 TiN sample before CV testing, and (d) the same sample after CV testing (−3.5 V to +3.5 V). While the coated sample shows lower surface degradation through corrosion than the noncoated one, HDPA-coating cannot eliminate corrosion on type 1 TiN samples.

obtained CV data. Bubble formation could be observed at all tested electrode surfaces with the naked eye. While we inhibited bubble formation by choosing a different solvent (section B below), corrosion could be eliminated by enhancing the self-passivating effect of titanium. Figure 7 reveals that the natural titanium oxide layer that is formed automatically on type 1 TiN samples in air does not provide enough passivation functionality to prevent surface corrosion. We performed a thermal oxidation step (450 °C, 5 h) on type 1 TiN samples to form a higher uniform titanium oxide layer and repeated the CV experiment as described above: corrosion results were similar to those shown in Figure 7. This can be explained by the fact that the porosity of naturally as well as thermally grown titanium oxide layers enables nonuniform selective oxidation.[16] Once a surface is initially selectively corroded due to passivation defects, corrosion will protrude also underneath surface areas with uncompromised passivation layers. Selective corrosion is known to be extremely destructive, especially at high potentials. In order to minimize porosity, we developed the custom-oxidation process described in subsection II.B yielding type 2 TiN samples carrying a highly uniform titanium oxide layer.

In a second step, we tested noncoated type 2 TiN samples using various SSA schemes (applied potential, 3−5 V; test duration, 5 min to 12 h; solvent, 1 mM KCl DI water). As opposed to results presented in Figure 7, no macroscopic corrosion was observed after the test. However, TEM cross-section images reveal that clusters of nanoscopic bubbles are formed and enclosed at the interface of the titanium oxide and TiN layers (Figure 8a,b). The higher the applied voltage, the more bubbles are formed. This effect can be explained as follows: When the applied potential of a test electrode in aqueous solution is moved from its redox equilibrium level toward more positive values, water dissociation (standard potential for oxidation is +1.229 V[6]) is facilitated at the surface of the electrode yielding an increasing number of free electrons in solution. Also, by applying more positive voltages to the test electrode the energy of the electrons is lowered, and some point electrons on solutes in the electrolyte will find an energetically more favorable state on the electrode and transfer there. This electron charge transfer is an oxidation current which according to the Nernst equation increases as the potential gets more positive. Transferred electrons are then nanoscopically corroding TiN underneath the titanium oxide layer[17] forming atomic Ti and N_2 with the latter being trapped between TiN and titanium oxide. Although the custom-developed titanium oxide layer successfully eliminates macroscopic corrosion of the TiN thin film electrode, it

(14) Fisher, G. B.; Gland, J. L. The interaction of water with the Pt(111) surface. *Surf. Sci.* **1980**, *94*(2−3), 446–455.
(15) Andersson, K.; Nikitin, A.; Pettersson, L. G. M.; Nilsson, A.; Ogasawara, H. Water dissociation on Ru(001): an activated process. *Phys. Rev. Lett.* **2004**, *93* (19), 196101–196104.
(16) Plieth, W. *Electrochemistry for materials science*, 1st ed.; Elsevier: London, 2008; ISBN 978−0-444−52792−9, pp 291ff.
(17) Saha, N. C.; Tompkins, H. G. Titanium nitride oxidation chemistry: an x-ray photoelectron spectroscopy study. *J. Appl. Phys.* **1992**, *72*, 3072–3079.

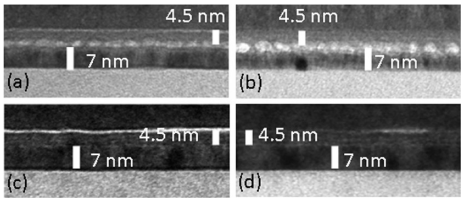

Figure 8. TEM cross-section images of (a) a noncoated type 2 TiN sample after SSA testing (3 V, 12 h, 1 mM KCl DI water solution), (b) another noncoated type 2 TiN sample after SSA testing (5 V, 5 min, 1 mM KCl DI water solution), (c) an HDPA-coated type 2 TiN sample before MSA testing (1 mM KCl 100% PEG-300 solvent), and (d) the same sample after MSA testing (test scheme according to Figure 5). The continuous bright line (c) and segments thereof (d) visible on top of the titanium oxide layer shows a chromium oxide layer added during TEM sample preparation. The coated sample (d) shows no TiN corrosion whatsoever at the interface of titanium oxide and TiN. The noncoated samples (a) and (b) show N_2 bubble formation at the top of the TiN layer. This is due to subsurface nanoscopic corrosion of TiN facilitated by electron charge transfer from the solution into the electrode. HDPA-coating reduces the hydroxyl functionality of the electrode surface and prevents nanoscopic corrosion. The increased N_2 content in samples (a) and (b) was also detected by XPS measurements.

does not completely passivate it. We shall see that HDPA-coating thus successfully eliminates nanoscopic TiN corrosion. Hence, HDPA-coating not only has a major impact on impeding water dissociation and bubble formation (subsection B below), but also plays an important role regarding corrosion protection by increasing the barrier to the transfer process.

In order to verify the statements of the previous paragraph and ultimately eliminate nanoscopic corrosion under working conditions of a DNA-Transistor, we tested HDPA-coated vs noncoated type 2 TiN samples for surface reaction effects performing the MSA scheme according to Figure 5 (7200 cycles, 14 h total run time, 6 h net exposure to both potential levels) in 1 mM KCl PEG-300 solution. Substituting water with poly(ethylene glycol) (PEG) or glycerol as solvents for the electrolyte has the following advantage: since PEGs and glycerol have only two end groups with hydroxyl functionality, the chance of electrolytic cleavage of the hydroxyl groups compared to water becomes much smaller, and therefore, the rate of oxidation at the electrode surface is significantly lessened. Figure 9 shows the monitored electrode surface current density over time. While essentially constant bilayer charging of the electrode surface can be measured for both potential states during the complete test time for HDPA-coated samples, a slight linear increase of surface reactivity is observed for noncoated samples. This is in perfect accordance with the observed nanoscopic corrosion of TiN under the surface: We could not detect this corrosion effect by means of AFM surface roughness monitoring (Figure 10) because the top surface of the titanium oxide layer remains unchanged throughout each test. Nevertheless, the TiN layer underneath is nanoscopically corroded increasing its surface roughness. Thereby the total oxidation surface area gradually increases, which in turn leads to increasing current densities for both potential levels. XPS measurements (data not shown) indicate a moderately increased N_2 content in the noncoated test sample after MSA testing as opposed to an unchanged N_2 content in tested HDPA-coated samples. Comparative TEM analysis showed no evidence of any subsurface N_2 bubble formation in HDPA-coated test samples (Figure 8c,d).

In summary, macroscopic corrosion of TiN thin film electrodes can be eliminated through the custom-developed titanium oxide layer, and nanoscopic subsurface corrosion can be eliminated by

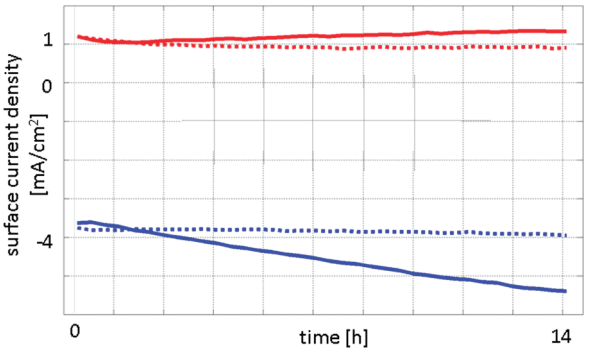

Figure 9. Surface current densities for HDPA-coated type 2 TiN samples (dotted lines) and noncoated type 2 TiN samples (solid lines) during MSA testing in 1 mM KCl 100% PEG-300 solution. Reductions currents (blue) are larger than oxidation currents (red). Coated samples show a continuous $t-i$ behavior indicating a bilayer-only charging effect on a constant electrode surface area. Linearly increasing oxidation and reduction current densities on noncoated test samples suggest that the surface of the test electrode is slightly increasing due to nanoscopic TiN corrosion during MSA testing as also discussed in Figure 8. The above data is another indicator showing that HDPA-coating successfully inhibits nanoscopic corrosion of TiN underneath the titanium oxide layer.

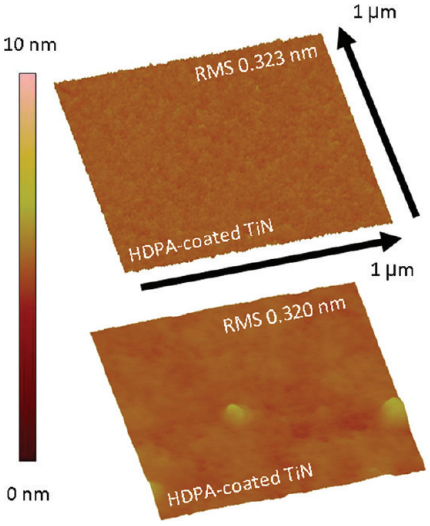

Figure 10. AFM surface roughness comparison of HDPA-coated type 2 TiN samples before (top) and after (bottom) MSA testing in 1 mM KCl 100% PEG-300 solution. The measurements reveal no change in surface roughness. Random impurities on tested samples (bottom) are residual salt colloids dried out on the electrode surface after testing. We could successfully remove these salt defects in an ultrasonic acetone bath (30 s, 21 °C).

HDPA-coating the titanium oxide surface. Test results prove that HDPA-coated type 2 TiN samples are completely resistant against macroscopic as well as nanoscopic corrosion under working conditions of a DNA-Transistor in operational mode.

B. Solvent Optimization. Substituting water by poly(ethylene glycol) (PEG) or glycerol as solvents for the electrolyte has several advantages. First, as already pointed out above, because PEGs and glycerol have very similar numbers of end groups with hydroxyl functionality but higher molecular weight than water, the chances of electrolytic cleavage of the PEG/glycerol hydroxyl groups compared to water become much smaller, and therefore, the rate of oxidation of the contacts is significantly retarded. The second advantage of PEG and glycerol over water is that they

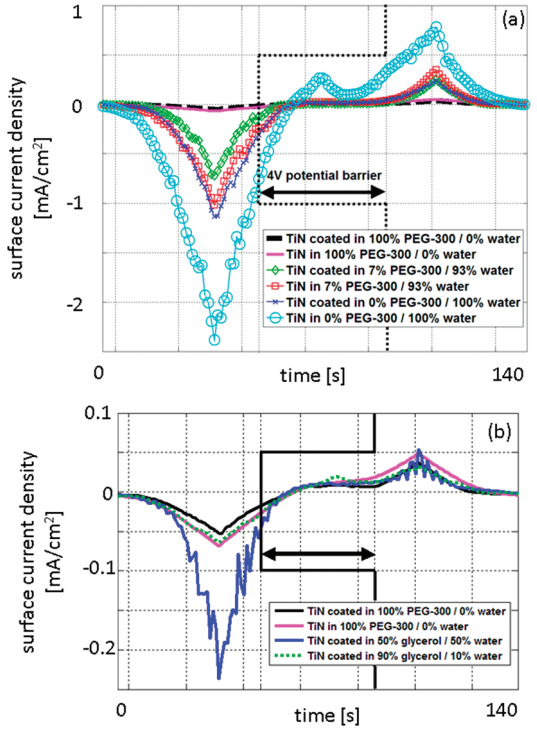

Figure 11. Cyclic voltamogramms for various aqueous 1 mM KCl glycerol and PEG-300 solutions and type 2 TiN samples: (a) CV proves that both, increasing PEG concentration in the solution and HDPA-coating the electrode surface decrease the intensity of electrochemical water dissociation at the electrode surface. (b) High-resolution cyclic voltamogramms of highly concentrated glycerol and PEG-300 solutions: no bubble formation at the electrode surface could be observed for noncoated type 2 TiN samples in 1 mM KCl 100% PEG-300 solution anymore (solid pink line). Hence, no bubble formation occurs for HDPA-coated type 2 TiN samples in 1 mM KCl 90% glycerol solution (dotted green line), which is a better solvent for DNA than PEG-based solutions.

both have much higher viscosities (pure glycerol approximately 1000×10^{-6} m^2 s^{-1}, pure PEG-300 approximately 60×10^{-6} m^2 s^{-1}) than water (1×10^{-6} m^2 s^{-1})[18,19] and therefore reduce the speed of DNA translocation through the nanopore, a very useful feature in the context of the DNA transistor device.

Increasing PEG or glycerol concentration in aqueous solutions gradually increases the effects explained above. Regarding the increase of viscosity, Segur and Oberstar[18] as well as Blazhnov et al.[20] have extensively studied the viscosity−concentration dependence in aqueous glycerol solutions. The model developed by Gonzaléz-Tello et al.[21] combined with density and viscosity data for PEGs[22,23] allows determination of the viscosity of aqueous PEG solutions for different PEG concentrations and molecular weights. Also, the water decomposition inhibiting effect of aqueous PEG and glycerol solutions becomes more dominant with increasing PEG or glycerol concentration because of the following mechanism: the common electroactive functionalities of water, PEG and glycerol evolve from their hydroxyl groups.

Although all three solvents have very similar numbers of O−H bonds in each molecule (water, PEG: 2, glycerol: 3), the number of O−H bonds per unit volume is significantly higher in water than glycerol, and in glycerol than PEG, respectively. This is due to the significant differences in molecular weight (MW) of the three materials (water 18 u, glycerol 92 u, PEG-300 average MW 300 u).

Furthermore, as explained in subsection II.C, adding an organic coating layer to the electrode surface renders it hydrophobic and thus not only contributes to corrosion protection but also suppresses water dissociation. This occurs because the water remains further away from the electrode surface, thereby exponentially reducing the probability of electron transfer via tunneling.

We evaluated a variety of aqueous 1 mM KCl glycerol and PEG-300 solutions with respect to the intensity of electrochemical dissociation they induce on HDPA-coated and noncoated type 2 TiN samples in a −2 V to +2 V voltage window using CV (Figure 11a). We choose 1 mM KCl because the proper functioning of our proposed DNA transistor (with pore diameters from 2 to 5 nm) depends on the penetration of the electrostatic field from the metal electrodes into the nanopore. This is facilitated by lower ionic concentration, which yields a larger Debye screening length. At 1 mM KCl concentration, the Debye screening length is around 10 nm, allowing the electric field to penetrate well into the nanopore. Low salt concentration is also desirable for other aspects of the DNA transistor. For example, single-stranded DNA is less prone to form secondary structure at lower ionic strengths,[24] and its persistence length increases with decreasing salt concentration.[25] We also investigated surface reactivity of type 2 TiN samples after adding 1 mM 0.1× TE buffer (1 mM Tris-HCl and 100 μM EDTA) to an aqueous 1 mM KCl solution. The buffered solution showed two major features: the surface reactivity level was slightly decreased for both redox reactions and oxidation suppression was significantly higher than reduction suppression. Detailed results of this buffer experiment are available as Supporting Information.

As for HDPA-coated samples, any corrosion is eliminated and all measured surface reactivity contributes exclusively to electrochemical dissociation. Furthermore, we showed by computational simulations[26] that coating a nanopore with a hydrophobic SAM has the effect of keeping a ssDNA molecule centered in the nanopore, a desirable effect for the DNA transistor. As for noncoated type 2 TiN samples, while bubble formation at the RDE sample surface could visually be observed in pure water solution and aqueous 7% PEG-300 solution, no bubble formation could be detected in 100% PEG-300 solution anymore. Hence, the surface reactivity intensity of a 100% PEG-300 solution may serve as target surface reactivity level where bubble formation in the solution is efficiently eliminated on noncoated type 2 TiN electrodes.

As expected, HDPA-coated samples showed lower surface reactivity than their noncoated counterparts in the same solvent. For more concentrated PEG-300 and glycerol solutions, the dissociation inhibition effect resulting from the PEG-300 and

(18) Segur, J. B.; Oberstar, H. E. Viscosity of glycerol and its aqueous solutions. *Ind. Eng. Chem.* **1951**, *43*(9), 2117–2120.
(19) Cruz, M. S.; Chumpitaz, L. D. A.; Guilherme, J.; Alves, L. F.; Meirelles, A. J. A. Kinematic viscosities of poly(ethylene glycols). *J. Chem. Eng. Data* **2000**, *45*, 61–63.
(20) Blazhnov, I. V.; Malomuzh, N. P.; Lishchuk, S. V. Temperature dependence of density, thermal expansion coefficient and shear viscosity of supercooled glycerol as a reflection of its structure. *J. Chem. Phys.* **2004**, *121*(13), 6435–6441.
(21) Gonzaléz-Tello, P.; Camacho, F.; Blázquez, G. Density and viscosity of concentrated aqueous solutions of polyethylene glycol. *J. Chem. Eng. Data* **1994**, *39*, 611–614.
(22) Mei, L.-H.; Lin, D.-Q.; Zhu, Z.-Q.; Han, Z.-X. Densities and viscosities of polyethylene glycol + salt + water systems at 20°C. *J. Chem. Eng. Data* **1995**, *40*, 1168–1171.
(23) Eliassi, A.; Modaress, H. Densities of poly(ethylene glycol) + water mixtures in the 218.15−328.15 K temperature range. *J. Chem. Eng. Data* **1998**, *43*, 719–721.
(24) Lang, B. E.; Schwarz, F. P. Thermodynamic dependence of DNA/DNA and DNA/RNA hybridization reactions on temperature and ionic strength. *Biophys. Chem.* **2007**, *131*, 96–104.
(25) Murphy, M. C.; Rasnik, I.; Cheng, W.; Lohman, T. M.; Ha, T. Probing single-stranded DNA conformational flexibility using fluorescence spectroscopy. *Biophys. J.* **2004**, 2530–2537.
(26) Luan, B.; Harrer, S.; Afzali, A.; Peng, H.; Waggoner, P.; Polonsky, S.; Stolovitzky, G.; Martyna, G.; Tribological Effects on DNA Translocation in a SAM-Coated Nanochannel. *J. Phys. Chem. B* **2010**, accepted for publication.

Table 1. Surface Current Densities Measured by CV for HDPA-Coated and Noncoated Type 2 TiN Samples in 1 mM KCl 100% DI Water vs 100% PEG-300 Solutions at the Boundaries of the 4 V Voltage Window[a]

applied voltage	$i_{100\%water}$ [mA/cm^2]	$i_{100\%PEG\text{-}300}$ [mA/cm^2]	HDPA-coated	inhibition factor
+2 V	0.015	0.003	yes (c)	5.0
−2 V	−0.22	−0.016	yes (c)	13.8
+2 V	0.099	0.013	no (nc)	7.6
−2 V	−0.66	−0.025	no (nc)	26.4
+2 V	0.099 nc	0.003 c	-	33.0
−2 V	−0.66 nc	−0.016 c	-	41.3

[a] Increasing PEG concentration as well as HDPA-coating inhibits surface reactivity significantly. In particular, substituting water by PEG-300 and HDPA-coating the sample decreases the oxidation current by a factor of 33.0 and the reduction current by a factor of 41.3, respectively. This decrease is enough to efficiently suppress electrode corrosion and bubble formation in the solution.

glycerol content, respectively, became dominant over dissociation inhibition due to HDPA-coating. Table 1 provides inhibition factors calculated for oxidation currents (applied potential +2 V) as well as reduction currents (applied potential −2 V) comparing HDPA-coated to noncoated type 2 TiN samples in 1 mM KCl DI water and 100% PEG-300 solution, respectively.

Dissolving DNA in aqueous PEG-solutions is challenging, since especially high-molecular-weight PEGs tend to induce colloid and gel formation of DNA molecules.[27−30] Aqueous glycerol solutions on the other side proved to be well-suited as solvents for DNA[31] and as medium for moving DNA molecules through a solid-state nanopore.[32]

Figure 11b shows that HDPA-coated type 2 TiN electrode samples in aqueous 90% glycerol solution show the same level of surface reactivity as noncoated type 2 TiN samples in the bubble-free 100% PEG-300 reference solution. Therefore, we conclude that aqueous 1 mM KCl 90% glycerol solution is to be chosen as the DNA solvent efficiently eliminating electrochemical dissociation and hence bubble formation.

V. Conclusion

We have studied the electrochemical surface reactivity characteristics of various thin film metal electrodes (noncoated TiN, noncoated plasma-oxidized TiN, HDPA-coated plasma oxidized TiN, noncoated Pt, noncoated Ru) in selected aqueous electrolyte−solvent systems (1 mM KCl DI water, aqueous 1 mM KCl PEG-300 solutions, aqueous 1 mM KCl glycerol solutions) with special focus on minimizing corrosion and water dissociation effects. A special plasma-oxidization process for passivating TiN thin films, as well as a process for coating such oxidized surfaces with a monolayer of HDPA to inhibit electrochemical dissociation, was developed. Both processes are optionally isotropically or anisotropically applicable to planar as well as angled or vertical surfaces and can thus be performed inside a nanopore.

All presented electrochemical tests were performed on planar nonpatterned electrode test samples and designed in such a way that all results should also hold in a real DNA-Transistor device environment. Our results show that custom plasma-oxidized, HDPA-coated TiN thin film electrodes and an aqueous 1 mM KCl 90% glycerol solution as DNA solvent constitute an electrochemically sound design for a DNA-Transistor device. Electrode corrosion as well as bubble formation inside the nanopore are essentially eliminated in this electrode−electrolyte−solvent system.[33]

The electrochemistry results presented in this paper constitute one crucial step forward toward implementing a working DNA-Transistor device. Subsequent steps in the development of the DNA transistor will include the development of sensing techniques for single-base readout while ssDNA is translocated through the nanopore. Our current work focuses on evaluating various sensing techniques using custom-built nanopore membranes incorporating the optimized electrochemical environment as presented in this paper.

Even though some of the parameters used in this work are motivated by the development of a DNA transistor, most of our results are applicable to a wide variety of systems in which nanoelectrodes are placed in an aqueous solution at electrochemistry-activating voltages.

Acknowledgment. The authors gratefully acknowledge the Materials Research Laboratory (MRL) at the IBM T. J. Watson Research Center, and especially Stephen A Brown, for assistance in preparing TiN thin films. We express our gratitude towards the following colleagues: Mark Reuter for assisting with performing AFM measurements, John A. Ott for TEM support, John B. Hannon for XPS measurements, George F. Walker for SEM support, and Stanislav Polonsky for discussions on current measurement data. Ajay Royyuru provided valuable advice. The work presented was supported by Award Number R01HG005110 from the National Human Genome Research Institute.

Supporting Information Available: Cyclic voltammetry measurement of type 2 TiN samples in 100% aqueous 1 mM KCl/1 mM 0.1x TE buffer (1 mM Tris-HCl and 100 μM EDTA) solution. This material is available free of charge via the Internet at http://pubs.acs.org.

(27) Paithankar, K. R.; Prasad, K. S. N. Precipitation of DNA by polyethylene glycol and ethanol. *Nucleic Acids Res.* **1991**, *19*(6), 1346.
(28) Kawakita, H.; Uneyama, T.; Kojima, M.; Morishima, K.; Masubuchi, Y.; Watanabe, H. Formation of glubules and aggregates of DNA chains in DNA/polyethylene glycol/monovalent salt aqueous solutions. *J. Chem. Phys.* **2009**, *131*, 094901–094909.
(29) Eliasson, R.; Hammarsten, E.; Lindahl, T.; Björk, I.; Laurent, T. C. The stability of deoxyrobonucleic acid in glycol solution. *Biochim. Biophys. Acta* **1963**, *68*, 234–239.
(30) Bloomfield, V. A. DNA condensation. *Curr. Opin. Struct. Biol.* **1996**, *6*, 334–341.
(31) Liang, D.; Song, L.; Chen, Z.; Chu, B. Effect of glycerol-induced DNA conformational change on the separation of DNA fragments by capillary electrophoresis. *J. Chromatogr., A* **2001**, *931*, 163–173.
(32) Fologea, D.; Uplinger, J.; Thomas, B.; McNabb, D. S.; Li, J. Slowing DNA translocation in a solid-state nanopore. *Nano Lett.* **2005**, *5*(9), 1734–1737.
(33) Harrer, S.; Waggoner, P. S.; Luan, B.; Afzali-Ardakani, A.; Goldfarb, D. L.; Peng, H.; Martyna, G.; Rossnagel, S. M.; Stolovitzky, G. A. Electrochemical protection of thin film electrodes in solid state nanopores. Submitted for publication, November 2010.